A new methodology exploring the record of snow avalanches in lake sediments

Laurent Fouinat[1], Pierre Sabatier[1], Jérôme Poulenard[1], Jean-Louis Reyss[2], Xavier Montet[3], Fabien Arnaud[1].

[1]EDYTEM, Université Savoie Mont Blanc, CNRS 73376 Le Bourget du Lac Cedex, France
[2]LSCE, Université de Versailles Saint-Quentin CEA-CNRS, avenue de la Terrasse, 91198 Gif-sur-Yvette cedex, France
[3]University of Geneva Department of Radiology and Medical Informatics Genève, Rue Gabrielle-Perret-Gentil 4, CH-1211, Switzerland

Correspondence to: Laurent Fouinat (laurent.fouinat@univ-smb.fr)

Abstract. In recent years, wet avalanche deposits have become a subject of increasing concern in a context of both global change and winter mountain tourism activities. This study focuses on the use of a new methodology based on CT scans to identify snow avalanche deposits in lake sediment. Here, we study the mid-elevation Lake Lauvitel system (western French Alps), which features steep slopes and avalanche corridors. CT scanning is a fast, non-destructive method based on X-ray technology and allows the assessment of relative density of clasts in the samples. We applied this method to sediment cores, leading to the 3D identification of the dense rocks that characterize wet avalanches. A total of eight periods of higher avalanche activity are identified since AD 1880 at the site. This new methodology is suitable for avalanche deposit reconstruction and may be applicable more widely in characterization of sedimentary archives alongside existing approaches.

1 Introduction

Snow avalanches are a natural hazard presenting great risks to mountain populations because of high transport competence and strong impact force (Blikra and Nemec, 1998). For most of wet avalanche, erosion occurs when the avalanche runs over bare ground or involves the whole thickness of the snow cover (Luckman, 1977). Two types are distinguished according to their water content, slush flows corresponding to a liquid mixture of mud and snow and wet avalanches described as non-water saturated snow flow moving as a solid mass composed of adjacent snow balls (Jomelli and Bertran, 2001). The mechanisms of erosion are various, abrasion, scratching and impact of the basal debris or even plucking unconsolidated rocks from the substratum; they can form distinctive geomorphic features such as narrow or funnel shaped gullies, debris covered slopes and small depression formed by repeated avalanche impacts called avalanche pits (Rapp, 1959; Luckman, 1977). In recent years, the number of wet avalanches has substantially increased due to warmer snow pack (Ancey and Bain, 2015). Their carrying capacity goes from smallest grains deposited by aeolian transport on the snow to large boulders (van Steijn et al., 1995; Blikra and Nemec, 1998; Jomelli et al., 2007; Sæmundsson et al., 2008; Van Steijn, 2011). Typical avalanches debris zones were described, in French Alps crystalline rocks, to be composed of a source area consisting of steep rock walls, a transitional area and a terminal lobe. The latter is characterized by an elevation between 600 and 2400 m a.s.l., close to 0°C annual isotherm and slopes comprised between 15-27° (Jomelli et al., 2011). Avalanche deposit stratigraphy is close to debris flow deposits, the difference being that the snow matrix melts shortly after deposition, and was described by (Blikra Nemec 1998) as unsorted, scattered clasts and gravel patches infield with waterlain sand or pebbly sand. The avalanches processes in mountain terrains are generally controlled by both climate such as temperature and rainfall activity (van Steijn et al., 1995; Jomelli et al., 2011; Van Steijn, 2011) and local slope conditions (Blikra and Nemec, 1998).

Reconstructing past avalanche dynamics in contexts of known climate changes could hence bring valuable new scientific data. Several studies exploring snow avalanche recurrence periods over the course of centuries to millennia in order to relate them to climate changes were led in particular in Norwegian lake sediment (Blikra and Nemec, 1998; Seierstad et al., 2002; Nesje et al., 2007; Vasskog et al., 2011). These studies focused on the outlier presence

of coarse particles in fine sediment. These coarse particles could have been incorporated into the sediment by different gravity transport processes e.g. i) related to liquid water such as high energy run off or debris flows competent enough to transport clay size to boulder size sediment ii) Rock fall transporting essentially sand to large boulders sediment but with low occurrence frequency iii) glaciers from clay to very large boulders iv) wet snow avalanches transporting clay size to gravel size sediment (Blair and McPherson, 1999; Vasskog et al., 2011). The incorporation of gravels transported to the lake will be different depending on the presence of ice. If lake is frozen the sediment would be deposited on top of the ice until thaw, then ice would spread around the lake and release clastic material falling to the lake bottom and creating drop stones (Luckman, 1975). If the lake is already freed from ice, the sediment would enter directly in the water creating a localized accumulation of sediment. In the case of debris flow, the resulted deposit was described as an underflow characterized by a normal gradation and well sorted sediments (Irmler et al., 2006). Another transport process non gravity related, would be particles trapped in ice on the lakeshore in the early winter, when ice melts in spring, the particles would be transported around lake surface then fall at the lake bottom as drop stones. To recover these coarse particles in the sediment cores, it is necessary to use a sieve to isolate, identify and count them, which is a destructive and time-consuming method. Several studies have explored snow avalanche records in the Alps based on dendrochronological reconstructions (Casteller et al., 2007; Corona et al., 2010; Corona et al., 2013). All of them were limited by the age of the trees in the avalanche paths. In France, the risk related to avalanches has been studied at a national scale since 1920 and has led to the "Enquête Permanente sur les Avalanches" (EPA) database, which records the number of avalanches in specific paths. Studies exploring this record through statistical analysis (Castebrunet et al., 2012; Eckert et al., 2013; Eckert et al., 2013b) have increased our understanding of snow avalanches and their relationship with climatological conditions. However, this requires a database composed of numerous records. There is thus a need to develop a new methodology to obtain continuous reconstructions of past avalanches. In this study, we explored the potential of CT scanning to identify snow avalanches record in lacustrine sediment. The main advantage of this technique is that it provides continuous and non-destructive analysis.

Over the last 50 years, X-ray radiographs were initially used to explore the internal structure of sediment cores (Bouma, 1964; Baker and Friedman, 1969) in order to optimize the opening process or even explore bioturbation structures in the sediment (Howard, 1968). One of the technical problems was the loss of information with respect to depth, as the radiographs are a plane representation of a 3D structure. In recent years, with improvements in X-ray technology, CT scanning has been used to identify the sedimentary imprints of river floods (Støren et al., 2010) and to explore sedimentary structures through 3D reconstructions (Pirlet et al., 2010; Bendle et al., 2015). A recent review of CT scans in the geosciences (Cnudde and Boone, 2013) demonstrates the growing application possibilities of this analysis as well as the limits of the technique. Furthermore, this review highlights the fact that this method has never been used to reconstruct past snow avalanches.

The exploration of CT scan analysis as a new tool aims to develop a simpler, faster and non-destructive methodology. We tested it on sediment cores from Lake Lauvitel located in the Oisans valley (western French Alps). This site has the advantage of presenting steep slopes with three avalanche corridors ending directly in the lake. Some avalanches have been observed in the spring, and snow accumulation is sometimes present at the base of the

corridors. This site is well suited to explore the reconstruction of an avalanche record based on avalanche deposits in a lacustrine sedimentary sequence.

2 Materials and methods

1.1 Study site

Lake Lauvitel (44° 58' 11.4"N, 6° 03' 50.5" E) is located 1500 m above sea level (a.s.l.) in the Oisans valley of the western French Alps, 35 km southeast of Grenoble. The lake covers an area of 0.35 km² and is 61 m deep, and the total drainage area is approximately 15.1 km². The lake was created after a large rockslide dated to 4.7±0.4 kyr ^{10}Be exposure age (Delunel et al., 2010). The natural permeable dam created after this event caused a change in lake level of approximately 20 m. Due to geomorphological settings, slopes around the lake are very steep and three avalanche corridors (C1, C2, and C3) are present on the western side of the lake (Fig. 1b). They are accompanied by the presence of snow accumulation at their bottom in spring (National Park ranger, Jérôme Forêt, pers. comm.), and avalanches have been observed in C1 (Fig. 1e). The watershed bedrock consists mainly of granite and gneiss, with minor outcrops of sedimentary rocks (Triassic limestone). The C1 track ends in an upper basin in the northern part of the lake, likely with no connection to the deeper part of the lake. C2 and C3 are located just above the coring location; there is no clear evidence of an obstacle preventing the sediment input from reaching the coring location. From the end of December to the beginning of May, the lake surface is frozen, and snow covers most of the watershed. The lake and its surroundings are situated in the Ecrins National Park restricted area.

Figure 1

1.2 Core description and methods

The core LAU11P2 (76 cm) was retrieved using a short UWITEC gravity corer to obtain a well-preserved interface, and LAU1104A (104.5 cm) was retrieved using a piston corer with a 90-mm sampling tube at the same location. The cores were split lengthwise and photographed at high resolution (20 pixels mm^{-1}). We examined in detail the visual macroscopic features of each core to define the different sedimentary facies to determine the stratigraphic correlation between the two cores.

CT scanning was performed at Hopitaux Universitaires de Genève (HUG) using a multidetector CT scanner (Discovery 750 HD, GE Healthcare, Milwaukee, Wis). The acquisition parameters were set as follows: 0.6-s gantry rotation time, 100 kVp, 0.984:1 beam pitch, 40-mm table feed per gantry rotation, and a z-axis tube current modulation with a noise index (NI) of 28 (min/max mA, 100/500) and a 64×0.625-mm detector configuration. All CT acquisitions were reconstructed with the soft tissue and bone kernel in order to enhance the density contrast (Tins, 2010). The images reconstructed with the bone kernel were used for subsequent analysis. The raw DICOMM images were converted to an 8-bit .TIFF format using Weasis (v2.0.3) viewer. The radiograph resolution is 512x512 pixels, with up to 256 grey scale values. In this study, the sediment core was divided into 1,045 1-mm-thick frames, each pixel corresponding to a resolution of up to 500x500 µm and thus a voxel of 0.25 mm^3. The images were then

stacked using the Image J FIJI application, and image treatments were performed using the 3D Object Counter plugin (Bolte and Cordelieres, 2006). First, we set a threshold to isolate the selected grey values, and we then applied a despeckle filter to remove the noise due to measurement. Finally 3D Object counter was used to reconstruct the particles and characterize them in a 3D coordinate system.

Grain size measurements were carried out on the core using a Malvern Mastersizer 800 particle-sizer at a lithology dependent sampling interval. Utrasonics were used to dissociate particles and to avoid flocculation. Several layers of gravel-sized mineralogic particles were identified (Fig. 2a) in the LAU1104 sediment core. To obtain a quantitative estimate of these particles, we passed samples through a 1-mm mesh and wet-sieved the sediment at variable intervals from 1 to 3 cm depending on the gravel concentration. The number of particles >2 mm and macro-remains present in the sieve were counted for each interval in the core LAU1104A.

The chronology of the Lake Lauvitel sediment sequence is based on short-lived radionuclide measurements. The short-lived radionuclides in the upper 75 cm of core LAU11P2 were measured using high-efficiency, very low-background, well-type Ge detectors at the Modane Underground Laboratory (LSM) (Reyss et al., 1995). The sampling intervals followed facies boundaries, resulting in a non-regular sampling of approximately 1 cm. Twelve thick beds (at depths of 10.4-12.7, 17.3-19, 22.9-24.8, 29.7-30.9, 38-39, 40.6-42.4, 43.1-44.2, 45.7-50, 54.5-56.9, 60.4-62.5, 64.1-66 and 67.2-68.3 cm) were not analyzed because they were considered to be instantaneous deposits or part of an instantaneous deposit (see Results). ^{210}Pb excess was calculated as the difference between total ^{210}Pb and ^{226}Ra activities.

3 Results

3.1 Lithostratigraphy

The core lithology is composed of three facies (Fig. 2a). Facies 1 (F1) is silty-clay, dark-brown, finely laminated layer. It is interbedded by two other facies that are almost always associated with each other: Facies 2 (F2) is a normally graded bed from coarse sand to silt, sometimes with an erosive base; this facies is always associated with a thin white clay-rich layer Facies 3 (F3) on the top. Fig. 2b presents typical normally graded beds with grain size distribution (in red) characterized by a median grain size (Q50) of 44.1 µm and a mode of 81 µm. F1 (in green) exhibits a median grain size of 13.5 µm and a mode of 11.9 µm. Sometimes, F1 presence coincides with coarse gravel in the sediment, then the median grain size is similar 9.7 µm, but two modes are discernible at 7.2 and 258 µm. Sorting reveals different values depending on the deposit type; 2.50 average in the normally graded beds, 2.65 for the annual sedimentation and 3.05 for annual sedimentation with gravel presence. The small difference in median grain size between annual sedimentation with and without gravel suppose limited addition in the fine grains fractions, but fraction superior to 100 µm and bad sorting and Q90 reveals a significant addition of sand size grains in the gravel layers. The presence of terrestrial macro-remains is sometimes identifiable in F2. A total of 18 normally graded beds are present in the core LAU1104A, with thicknesses ranging from 0.7 to 13 cm. The evolution of the median grain size and the coarser 10th percentile along the graded bed allows us to consider them to be turbidites caused by heavy rainfall in the watershed (Støren et al., 2010; Giguet-Covex et al., 2012; Wilhelm et al., 2012b,

2012ba, 2013; Gilli et al., 2013; Wilhelm et al., 2015). We did not observe a typical avalanche deposit facies in the split core. Sometimes, rare millimeter- to centimeter-scale grains are present in the turbidite deposits, but they are unlikely to have originated from the torrential activity due to the distance from the delta. In addition, the gravels are situated in the upper part of the flood deposit, corresponding to receding torrential activity. The presence of gravel in the turbidites is interpreted to be the result of extreme rainfall triggering a flood and activating a debris flow in the avalanche corridor or simply transporting unconsolidated rocks from the steep slopes to the coring location.

The CT scan analysis is based on relative density. The histogram (Fig. 3a) represents the frequency of each of 1-255 levels of grey (0 is not shown on the graph due to overrepresentation corresponding to the background signal). Three modes representing the most frequent values are apparent in the histogram; they must be associated with certain types of sediment. The first mode is centered on the 106 value. After selecting this mode, we isolated the numerical values in order to map them by using the plugin, the corresponding elements in the sediment core were organic matter (OM) small macroremains, such as a pinus twig found at 58 cm of depth (Fig. 3-e1). We thus selected the 95-125 range to identify OM. The second mode, centered on the 174 value, is relatively denser than OM. Its large spectrum and high count values correspond to the most common element in the sediment core, which would be the silty clay sedimentation matrix (Fig. 3b). The last mode is essentially the 255 level of grey. Because it is the densest value possible, it corresponds to denser elements present in the silty-clay matrix. We selected the 240-255 value range and isolated them, and searched for corresponding particles in the sediment core. We identified gravel-sized granite elements in the sediment core (Fig. 3-e3-e4).

To compare objects counted numerically and objects counted manually, we need to know the size limit in units of volume (voxels), which is equivalent to 2-mm-diameter holes in a sieve. In 2D, a particle is retained in the sieve only if at least two sides are 2 mm in length, meaning at least two sides are 4 pixels long. Therefore, a particle of 16 (4x4) pixels with four sides that are 2 mm long will be retained in the sieve. However, if the same particle is missing 1 corner (minus three pixels, corresponding to a particle of 13 pixels), the particle would still be large enough to be retained in the sieve. This angular shape is more likely to be encountered in avalanche deposits; thus, we set the size limit of the 3D Object Counter plugin to 13 pixels, which corresponds to 13 voxels. The organic macroremains are composed of herbs, twigs or even roots, and their shapes were very complicated. Therefore, we did not choose any volume limit in their identification process.

In the LAU1104A sediment core, a total of 499 gravel clasts equal to or larger than 13 voxels were identified. The largest high-density object recovered from the core LAU1104A was an angular piece of granite of over 6 centimeter on its longest side and weighing 206.03 g. Considering a volumetric mass density of 2.7 t/m^3, its volume can be estimated to be 76 307 mm^3 ($\rho=m/V$). In comparison, the numerical volume is estimated to be 382,293 voxels, corresponding to 92,073 mm^3. Thus, a difference of +17% in the volume for the CT counting is observed, probably due to pixel resolution. The volume is thus overestimated, but still close to the actual rock volume.

We then compared the 3D Object Counter results and the coarse grains recovered from the sediment cores in slices of variable thickness ranging from 1 to 3 cm. The depth 97-98 cm had no gravel > 2 mm in either the manual or numerical counting (Fig. 3b, d). When considering a large amount of gravel, the manual and numerical counting methods showed differences. For depths 15-18, 42-44, 44-46, 51-52, and 72-73 cm, the number of gravel clasts was always underestimated by the numerical counting. As the 3D Object Counter plugin is identifying objects from one

pixel and its 8 neighbours in 2D and its 26 neighbours in 3D (Bolte and Cordelieres, 2006), the identification of objects could vary, especially because of the noise treatment and when the object size is close to the image resolution. The numerical counting result is slightly underestimated compared to the manual counting result (30% on average). The depths 5-7 and 46-48 cm, on the contrary, showed an overestimation by the numerical counting (77% on average). Considering the resolution, it is possible that a certain number of aggregated sand grains could have been considered gravel by the numerical counting method, leading to an overestimation. This could be explained by the presence of flood deposits in these two depths (Fig. 3b). Aggregated sand-sized elements would be considered by numerical counting as larger elements, and the sand-sized elements are rounder and would go through the sieve, as opposed to an angular particle of similar volume, which would be retained in the sieve. Overall, from this comparison between the numerical and the manual counting and accounting for the previously mentioned CT scan bias, we obtained a relatively well-constrained positive correlation (r=0.79, n=8; p-value=0.0077) (Fig. 3d).

The OM counting identified 7,413 objects, spread throughout almost every part of the sediment core. The largest OM element found in the core was 6,949 voxels in size, corresponding to 1,732 mm^3. This OM element was situated at a depth of 58 cm in the middle of a flood deposit (Fig. 3b) and was identified as a pinus tree twig (Fig. 2e-1). In total, 89.2% of the numerically counted elements are under 3.25 mm^3 (13 voxels), and almost every element recovered in the sieve corresponded to small leafs, roots, twigs or herb macroremains (Fig. 3e-2).

Figure 2

3.3 Chronology

The ^{210}Pb excess profile (Fig. 4) showed a regular decrease punctuated by drops in $^{210}Pb_{ex}$ activities. Following (Arnaud et al., 2002), these low values of $^{210}Pb_{ex}$ were excluded to construct a synthetic sedimentary record, because these values are related to F2/F3 facies association, which is considered to be instantaneous turbidite deposits. Plotting on a logarithmic scale, the $^{210}Pb_{ex}$ activities revealed a linear trend (Wilhelm et al., 2012b). Applying the CFCS model (Goldberg, 1963), we obtain a mean accumulation rate of 3.7 +/- 0.3 mm yr^{-1}. The uncertainty in the sedimentation rate was derived from the standard error of the CFCS model linear regression. Ages were then calculated using the CFCS model applied to the original sediment sequence to provide a continuous age-depth relationship. In addition, ^{137}Cs and ^{241}Am activity profiles present two peaks and one peak, respectively. The older peak in ^{137}Cs activity at 28.1 cm is contemporary with the peak in ^{241}Am activity, allowing us to associate it to the peak of nuclear weapons testing in the northern hemisphere in 1963. The younger peak in ^{137}Cs activity at 17.3 cm can be attributed to fallout from the Chernobyl accident in 1986 (Appleby et al., 1991). These two artificial peaks are in good agreement with the CFCS model (Fig. 4). In addition, we compared the historical flood calendar from the Vénéon river valley from the RTM-ONF data base (http://rtm-onf.ifn.fr/) to the instantaneous deposits recovered from the lake sediment for the last 100 years. In local archives, eight major flood events occurred in 2008, 2003, 1987, 1962, 1955, 1938, 1922 and 1914, could be correlated to the most important and recent graded deposits at depths of 0.4-2.9, 9.9-11.4, 18.7-20.1, 28.5-32.9, 38.2-39.6, 46-61, 64.9-66.7, and 67.7-69.1 cm, respectively. The good agreement between these independent chronological markers and the $^{210}Pb_{ex}$ ages strongly supports our age-

depth model for the last century and validates our interpretation that the F2/F3 facies correspond to instantaneous flood deposits.

Figure 3

4 Discussion

We did not find any specific facies related to the avalanches deposits, as opposed to the floods deposits. The grain size analysis reveals a specific distribution concerning facies F2 representing the annual sedimentation. Sometimes gravel size sediment are present in the annual sedimentation, in this case the grain size distribution exhibits an additional mode in the sand class, almost no changes in the silt class and higher sorting values. The OM presence in the lake sediment is an addition of terrestrial and in situ origin, based on the CT-scan analysis there is no clear relation between OM and gravel layers except maybe in the thickest gravel accumulation (Fig. 3b-5). Jomelli and Bertran, (2001) observed the fine sediment associated to an avalanche is representing 6-16% of total sediment, which would explain why we have difficulty identifying them at the same depth as gravel elements. The largest OM element observed was located at the base of the thickest flood deposit (Fig. 3b-1), thus OM is not a distinctive parameter to identify an avalanche deposit. The grain size analysis in the same thick flood deposit revealed that the Q90 was still lower than coarsest grains in the gravel layers, despite the presence of few coarse elements in the upper part of the flood deposit (Fig.2a). Their presence may be explained by smaller intermittent tributaries activated by rainfall, such as in the avalanches corridors, transporting coarse grains to the lake bottom through a debris flow process or just by unconsolidated rocks transport on the steep slopes. Both floods and debris flows are characterized by the presence of a clay/silt sediment fraction and by normally graded lacustrine deposits well sorted (Gilli et al., 2013; Irmler et al., 2006) as opposed to a multi modal grain size distribution with high sorting values with no gradation as observed in lacustrine avalanches deposits in Norway (Vasskog et al., 2011). The deposits exhibiting those characteristics with the addition of gravel elements observed by the CT-scan analysis are interpreted as pure avalanche deposits for Lake Lauvitel. In order to identify only avalanches, we do not consider gravel elements present in the graded deposits. The organic matter is usually associated with the fine sediment in an avalanche deposit, but the CT-scan analysis based on relative lower densities attributed to organic matter are not always coinciding with avalanche deposits. Only the thickest gravel accumulation shows clear increase of organic matter content as well as increase in gravel number. The organic matter income is also related to torrential activity, as observed in the (Fig. 3b-1) where a pinus twig was found. Fine lamination (F1) is present in the split sediment core despite of the presence of gravel-sized elements, which is remarkable considering the volume of the gravel class and the deposition on the lake bottom. Two possible explanations would be i) integration of gravel elements without any sediment disturbance or ii) the spring avalanche would be deposited on the top of the sediment-water interface, then the summer and autumn finely laminated sediment would be deposited posterior to the gravel and sand clasts and

filling the spaces between gravels. In any case, the basal deposit level would then represent the date of the avalanche deposit.

Wet avalanches occur at spring season when the snow pack is becoming unstable due loss of cohesion in the structure caused by warmer temperatures. It is also thaw season for lake ice. Hence, the avalanches could either be deposited on ice or enter directly in the water, as observed during the May 1st 2015 avalanche. At that time, the snow flow originated from the C1corridor in the northern part of the lake where an upper basin is present. It is likely to have no sedimentary connection with the deeper basin where the coring point is located. If the avalanche was deposited on lake ice, sediment may have been dispersed in the deeper basin as ice rafted debris and thus be recorded in a sedimentary core. Snow avalanche materials can be integrated into lacustrine sediments in two ways. In the case of a frozen lake, surface avalanche deposits are spread across the ice and subsequently drop to the lake sediment from drifting ice. When an avalanche occurs while the lake is ice-free, the avalanche deposits directly enter the water, and particles are concentrated in a more restricted area closer to the avalanche corridor. As this is a very local phenomenon, the coring point has to be directly beneath the avalanche corridor to record the maximum number of events, thus capturing both drop stones and direct avalanche deposits. An avalanche deposit would be identified as multiple gravel elements at the same sediment depth, as opposed to a single element that could be related to a single rock falling from steep slopes. In order to comprehend this deposition processes, multiple cores spatially dispersed in the deeper lake basin would give a better overall estimation.

Limits of counting: The numerical counting method using the CT scan radiographs is well suited for this type of study because density differences between fine lacustrine sediments and coarse gravel is quite significant. The centimeter-sized gravels found in sediment cores are also well suited to the resolution of the CT scan, especially because the analysis of a volume as large as the more than one-meter-long sediment core allows for a pixel resolution of only 500x500 µm. The good correspondence between the manual and numerical counting with respect to the absence of gravel-sized element in the sediment should be highlighted. Additionally, the largest elements are well identified, but smaller ones are more difficult to distinguish, as they are too close to the pixel resolution. This is the case for organic matter, which was identified in the sediment core (Fig.2b-2), mainly composed of small roots or leaves characterized by an elongated and thin shape, making them difficult to clearly identify with the CT-scan analysis, at least with the used resolution. Discrepancies between the manual and numerical counting are hence quite important and probably related to the image resolution. Thus, this study is limited to the presence of multiple gravel-sized elements in the sediment core. On solid ground, the presence of more than one gravel-sized element along with organic macroremains is interpreted as a snow avalanche deposit (Jomelli and Bertran, 2001; Nesje et al., 2007). In this context, the image resolution is precise enough to identify coarse-grained layers but is not good enough to precisely characterize each grain, especially the smallest ones and small organic matter. The CT scan is a powerful non-destructive tool for investigating the presence of coarse gravel-sized elements inside lacustrine sediment cores. In addition, identification of OM rich levels could be a good way to identify precise depths suitable for macro remains sampling for ^{14}C analysis. For further analysis of sedimentary elements, some calibration of known elements would be necessary. The density differences between different rock types or different organic macroremains do not allow further interpretation.

Figure 4

When applying the age model to the LAU1104A sediment core, we are able to express the number of rocks identified since AD 1880 (Fig. 5) per 5-mm slice. The number goes from zero to almost twenty gravel elements per 5 mm deposited in the lake floor. Possible avalanche deposits would be related to various gravel accumulation as the deposition of avalanches can occur on lake ice or directly in the water. However, a total of 499 gravel elements were identified in the sediment core, income is thus related to a frequent mechanism transporting them to the lake. In order to identify possible deposits we compared the number of gravel with historic records of winters with higher avalanche activity in the Oisans valley. The winter of 1922-1923 was an exceptional year in terms of winter precipitation in the Oisans valley, and avalanches destroyed numerous buildings and covered roads with thick snow deposits (Allix, 1923). The winter of 1969-1970 was also exceptional in terms of heavy snowfall, and no less than 800 avalanches were reported (Jail, 1970). On February 10th, 1970, an avalanche killed 39 people, making it the most catastrophic avalanche in the last 200 years. In 1978, the Ecrins National Park rangers reported numerous avalanches in the Oisans valley, especially in spring with wet snow avalanches temporarily blocking roads (Ecrins national park internal report, 1978). The avalanche activity in the French Alps has also been explored based on the EPA since 1950. Four periods correspond to higher snow avalanche frequency in the northern French Alps: 1950-1955, 1968-1970, 1978-1988, and 1993-1998 (Eckert et al., 2013) (Fig. 5). Comparison with an avalanche record based on tree rings located 10 km north from Lake Lauvitel in the Romanche river valley (Corona et al., 2010) is also presented in (Fig. 5). In the Lake Lauvitel sediment sequence, the periods of increased numbers of rocks are 1888, 1898, 1920-1931, 1939, 1949, 1970-1972, 1977-1980 and 1990-1993. These periods correspond roughly to higher avalanche activity in the previously mentioned records. The Romanche valley avalanche record exhibits numerous events during the AD 1920-1940 and 1970-1995, and no events since were recorded, as well as low number of rocks in Lake Lauvitel. They also correspond to periods of four or more coarse particles present in the sediment core (5 mm slices) (Fig. 5). This gravel limit number seems to correspond at least to major avalanche events recorded in the valley, despite the variability in the deposition (ice or water), the various exposures of avalanche corridors, and various analytical measurements. We thus set four rocks as the minimum for recording wet avalanche deposits in Lake Lauvitel as a non-exhaustive identification, constituting first avalanche record in lake sediments for the French Alps.

In Norway, similar avalanches in lake studies have been mostly related to winter precipitation (Seierstad et al., 2002; Nesje et al., 2007; Vasskog et al., 2011), and this phenomenon was more frequent during cold periods, such as the Younger Dryas or the Little Ice Age (Blikra and Nemec, 1998). In the French Alps, the correlation between winter precipitation and avalanche deposits seem probable (Corona et al., 2010), but due to the low quantity of information and the strong inter-annual variability in precipitation, it is quite difficult to reach solid conclusions regarding this relationship. To study this relationship, we need to develop long-term reconstructions of snow avalanche deposits, and the CT scanning method allows us to do this for longer sediment archives.

One of the advantages of the CT scans and the 3D Object Counter (FIJI) is that each element identified as an object is also characterized by x, y, z coordinates in the sediment core. We consider that with this methodology various coarse grains gravity transport mechanisms can be explored in e.g. lake sediments and it opens new perspective for further natural archives studies.

5 Conclusion

CT scans are a well-developed analysis in the medical community and have been used for several geoscience-related studies in the past decades. The principle of the analysis is based on differences in the relative densities of an object. This study explores the possibility of using this technique on a lake sediment core to reconstruct a past snow avalanche record. The analysis highlighted the presence of denser >2-mm mineralogical particles in the silty sedimentary matrix, as well as the abundant organic matter, which could be a useful tool for sampling macroremains for ^{14}C analysis. Both of these features are typical of wet snow avalanche deposits, and a total of three avalanches corridors are oriented directly into the western side of Lake Lauvitel. We interpreted the presence of both >2-mm particles and organic matter deposited into the lake as a proxy for snow avalanche events. This methodology opens new avenues for reconstructing past snow avalanche chronicles from lake sediment and for understanding avalanche variability in regard to past and modern climate changes.

6Acknowledgments

L. Fouinat's PhD fellowship was supported by a grant from Ecrins National Park, Communauté des Communes de l'Oisans, Deux Alpes Loisirs and the Association Nationale de la Recherche et de la Technologie (ANRT). The authors wish to thank Ecrins National Park for their authorization for sampling and assistance during the field work. The authors thank the Laboratoire Souterrain de Modane (LSM) facilities for the gamma spectrometry measurements and Hopitaux Universitaires de Genève (HUG) for the CT scan analysis.

References

Allix, A., 1923. Les avalanches de l'hiver 1922-1923 en Dauphiné. Rev. Géographie Alp. 11, 513–527. doi:10.3406/rga.1923.5519

Ancey, C., Bain, V., 2015. Dynamics of glide avalanches and snow gliding: Glide avlanches and snow gliding. Rev. Geophys. 53, 745–784. doi:10.1002/2015RG000491

Appleby, P.G., Richardson, N., Nolan, P.J., 1991. 241Am dating of lake sediments, in: Smith, J.P., Appleby, P.G., Battarbee, R.W., Dearing, J.A., Flower, R., Haworth, E.Y., Oldfield, F., O'Sullivan, P.E. (Eds.), Environmental History and Palaeolimnology, Developments in Hydrobiology. Springer Netherlands, pp. 35–42.

Arnaud, F., Lignier, V., Revel, M., Desmet, M., Beck, C., Pourchet, M., Charlet, F., Trentesaux, A., Tribovillard, N., 2002. Flood and earthquake disturbance of 210Pb geochronology (Lake Anterne, NW Alps). Terra Nova 14, 225–232.

Baker, S.R., Friedman, G.M., 1969. A non-destructive core analysis technique using X-rays. J. Sediment. Res. 39, 1371–1383. doi:10.1306/74D71E2E-2B21-11D7-8648000102C1865D

Bendle, J.M., Palmer, A.P., Carr, S.J., 2015. A comparison of micro-CT and thin section analysis of Lateglacial glaciolacustrine varves from Glen Roy, Scotland. Quat. Sci. Rev. 114, 61–77. doi:10.1016/j.quascirev.2015.02.008

Blair, T.C., McPherson, J.G., 1999. Grain-size and textural classification of coarse sedimentary particles. J. Sediment. Res. 69, 6–19.

Blikra, Nemec, 1998. Postglacial colluvium in western Norway: depositional processes, facies and palaeoclimatic record. Sedimentology 45, 909–959. doi:10.1046/j.1365-3091.1998.00200.x

Bolte, S., Cordelieres, F.P., 2006. A guided tour into subcellular colocalization analysis in light microscopy. J. Microsc. 224, 213–232.

Bouma, A.H., 1964. Notes on X-ray interpretation of marine sediments. Mar. Geol. 2, 278–309.

Castebrunet, H., Eckert, N., Giraud, G., 2012. Snow and weather climatic control on snow avalanche occurrence fluctuations over 50 yr in the French Alps. Clim. Past 8, p–855.

Casteller, A., Stöckli, V., Villalba, R., Mayer, A.C., 2007. An evaluation of dendroecological indicators of snow avalanches in the Swiss Alps. Arct. Antarct. Alp. Res. 39, 218–228.

Cnudde, V., Boone, M.N., 2013. High-resolution X-ray computed tomography in geosciences: A review of the current technology and applications. Earth-Sci. Rev. 123, 1–17. doi:10.1016/j.earscirev.2013.04.003

Corona, C., Georges, R., Jérôme, L.S., Markus, S., Pascal, P., 2010. Spatio-temporal reconstruction of snow avalanche activity using tree rings: Pierres Jean Jeanne avalanche talus, Massif de l'Oisans, France. CATENA 83, 107–118. doi:10.1016/j.catena.2010.08.004

Corona, C., Saez, J.L., Stoffel, M., Rovera, G., Edouard, J.-L., Berger, F., 2013. Seven centuries of avalanche activity at Echalp (Queyras massif, southern French Alps) as inferred from tree rings. The Holocene 23, 292–304. doi:10.1177/0959683612460784

Eckert, N., Keylock, C.J., Castebrunet, H., Lavigne, A., Naaim, M., 2013. Temporal trends in avalanche activity in the French Alps and subregions: from occurrences and runout altitudes to unsteady return periods. J. Glaciol. 59, 93–114. doi:10.3189/2013JoG12J091

Eckert, N., Lavigne, A., Castebrunet, H., Giraud, G., Naaim, M., 2013. Recent changes in avalanche activity in the French Alps and their links with climatic drivers: an overview, in: International Snow Science Workshop (ISSW). Irstea, ANENA, Meteo France, p. p–1211.

Giguet-Covex, C., Arnaud, F., Enters, D., Poulenard, J., Millet, L., Francus, P., David, F., Rey, P.-J., Wilhelm, B., Delannoy, J.-J., 2012. Frequency and intensity of high-altitude floods over the last 3.5ka in northwestern French Alps (Lake Anterne). Quat. Res. 77, 12–22. doi:10.1016/j.yqres.2011.11.003

Gilli, A., Anselmetti, F.S., Glur, L., Wirth, S.B., 2013. Lake sediments as archives of recurrence rates and intensities of past flood events, in: Dating Torrential Processes on Fans and Cones. Springer, pp. 225–242.

Goldberg, E.D., 1963. Geochronology with 210Pb. Radioact. Dating 121–131.

Howard, J.D., 1968. X-ray radiography for examination of burrowing in sediments by marine invertebrate organisms. Sedimentology 11, 249–258.

Irmler, R., Daut, G., Mäusbacher, R., 2006. A debris flow calendar derived from sediments of lake Lago di Braies (N. Italy). Geomorphology 77, 69–78. doi:10.1016/j.geomorph.2006.01.013

Jail, M., 1970. Note sur l'hiver remarquable 1969-1970 dans les Alpes françaises. Rev. Géographie Alp. 58, 505–513. doi:10.3406/rga.1970.3495

Jomelli, V., Bertran, P., 2001. Wet snow avalanche deposits in the French Alps: structure and sedimentology. Geogr. Ann. Ser. Phys. Geogr. 83, 15–28.

Jomelli, V., Brunstein, D., Grancher, D., Leone, F., Pavlova, I., Chenet, M., Utasse, M., 2011. Are Debris Floods and Debris Avalanches Responding Univocally to Recent Climatic Change-A Case Study in the French Alps. INTECH Open Access Publisher.

Jomelli, V., Delval, C., Grancher, D., Escande, S., Brunstein, D., Hetu, B., Filion, L., Pech, P., 2007. Probabilistic analysis of recent snow avalanche activity and weather in the French Alps. Cold Reg. Sci. Technol. 47, 180–192.

Luckman, B., 1977. The geomorphic activity of snow avalanches. Geogr. Ann. Ser. Phys. Geogr. 31–48.

Luckman, B., 1975. Drop stones resulting from snow-avalanche deposition on lake ice. J. Glaciol. 14, 186–188.

Nesje, A., Bakke, J., Dahl, S.O., Lie, O., Boe, A.-G., 2007. A continuous, high-resolution 8500-yr snow-avalanche record from western Norway. The Holocene 17, 269–277. doi:10.1177/0959683607075855

Pirlet, H., Wehrmann, L.M., Brunner, B., Frank, N., Dewanckele, J., Van Rooij, D., Foubert, A., Swennen, R., Naudts, L., Boone, M., Cnudde, V., Henriet, J.-P., 2010. Diagenetic formation of gypsum and dolomite in a cold-water coral mound in the Porcupine Seabight, off Ireland: Diagenetic gypsum in a cold-water coral mound. Sedimentology 57, 786–805. doi:10.1111/j.1365-3091.2009.01119.x

Rapp, A., 1959. Avalanche Boulder Tongues in Lappland. Geogr. Ann. 41, 34–48.

Reyss, J.-L., Schmidt, S., Legeleux, F., Bonté, P., 1995. Large, low background well-type detectors for measurements of environmental radioactivity. Nucl. Instrum. Methods Phys. Res. Sect. Accel. Spectrometers Detect. Assoc. Equip. 357, 391–397. doi:10.1016/0168-9002(95)00021-6

Sæmundsson, Þ., Decaulne, A., Jónsson, H.P., 2008. Sediment transport associated with snow avalanche activity and its implication for natural hazard management in Iceland, in: International Symposium on Mitigative Measures against Snow Avalanches. pp. 137–142.

Seierstad, J., Nesje, A., Dahl, S.O., Simonsen, J.R., 2002. Holocene glacier fluctuations of Grovabreen and Holocene snow-avalanche activity reconstructed from lake sediments in Grningstlsvatnet, western Norway. The Holocene 12, 211–222. doi:10.1191/0959683602hl536rp

Støren, E.N., Dahl, S.O., Nesje, A., Paasche, Ø., 2010. Identifying the sedimentary imprint of high-frequency Holocene river floods in lake sediments: development and application of a new method. Quat. Sci. Rev. 29, 3021–3033. doi:10.1016/j.quascirev.2010.06.038

Tins, B., 2010. Technical aspects of CT imaging of the spine. Insights Imaging 1, 349–359. doi:10.1007/s13244-010-0047-2

Van Steijn, H., 2011. Stratified slope deposits: periglacial and other processes involved. Geol. Soc. Lond. Spec. Publ. 354, 213–226. doi:10.1144/SP354.14

van Steijn, H., Bertran, P., Francou, B., Texier, J.-P., Hétu, B., 1995. Models for the genetic and environmental interpretation of stratified slope deposits: Review. Permafr. Periglac. Process. 6, 125–146. doi:10.1002/ppp.3430060210

Vasskog, K., Nesje, A., Storen, E.N., Waldmann, N., Chapron, E., Ariztegui, D., 2011. A Holocene record of snow-avalanche and flood activity reconstructed from a lacustrine sedimentary sequence in Oldevatnet, western Norway. The Holocene 21, 597–614. doi:10.1177/0959683610391316

Wilhelm, B., Arnaud, F., Sabatier, P., Crouzet, C., Brisset, E., Chaumillon, E., Disnar, J.-R., Guiter, F., Malet, E., Reyss, J.-L., Tachikawa, K., Bard, E., Delannoy, J.-J., 2012b. 1400years of extreme precipitation patterns over the Mediterranean French Alps and possible forcing mechanisms. Quat. Res. 78, 1–12. doi:10.1016/j.yqres.2012.03.003

Wilhelm, B., Arnaud, F., Sabatier, P., Crouzet, C., Brisset, E., Chaumillon, E., Disnar, J.-R., Guiter, F., Malet, E., Reyss, J.-L., Tachikawa, K., Bard, E., Delannoy, J.-J., 2012b. 1400years of extreme precipitation patterns over the Mediterranean French Alps and possible forcing mechanisms. Quat. Res. 78, 1–12. doi:10.1016/j.yqres.2012.03.003

Wilhelm, B., Arnaud, F., Sabatier, P., Magand, O., Chapron, E., Courp, T., Tachikawa, K., Fanget, B., Malet, E., Pignol, C., Bard, E., Delannoy, J.J., 2013. Palaeoflood activity and climate change over the last 1400 years recorded by lake sediments in the north-west European Alps. J. Quat. Sci. 28, 189–199. doi:10.1002/jqs.2609

Wilhelm, B., Sabatier, P., Arnaud, F., 2015. Is a regional flood signal reproducible from lake sediments? Sedimentology 62, 1103–1117. doi:10.1111/sed.12180

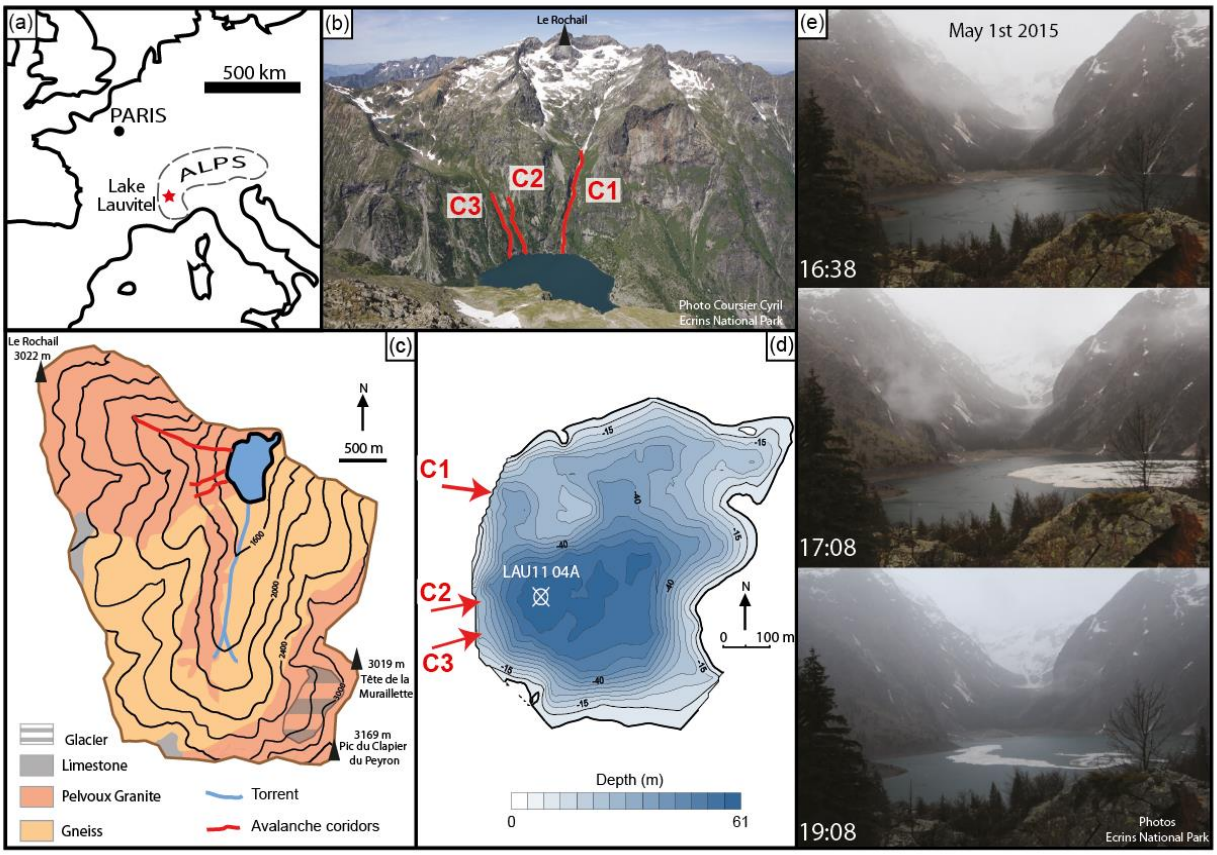

505 **Figure 1: (a) Location of Lake Lauvitel, (b) Photo looking westward toward the location of the three avalanche corridors in the Lake Lauvitel watershed. (c) Simplified geologic map of the Lake Lauvitel watershed. (d) Lake Lauvitel bathymetric map and location of the three avalanche corridors and position of the LAU1104A coring point. (e) Photos of the lake looking to the south, with an avalanche entering the lake via the C1 corridor on May 1st 2015.**

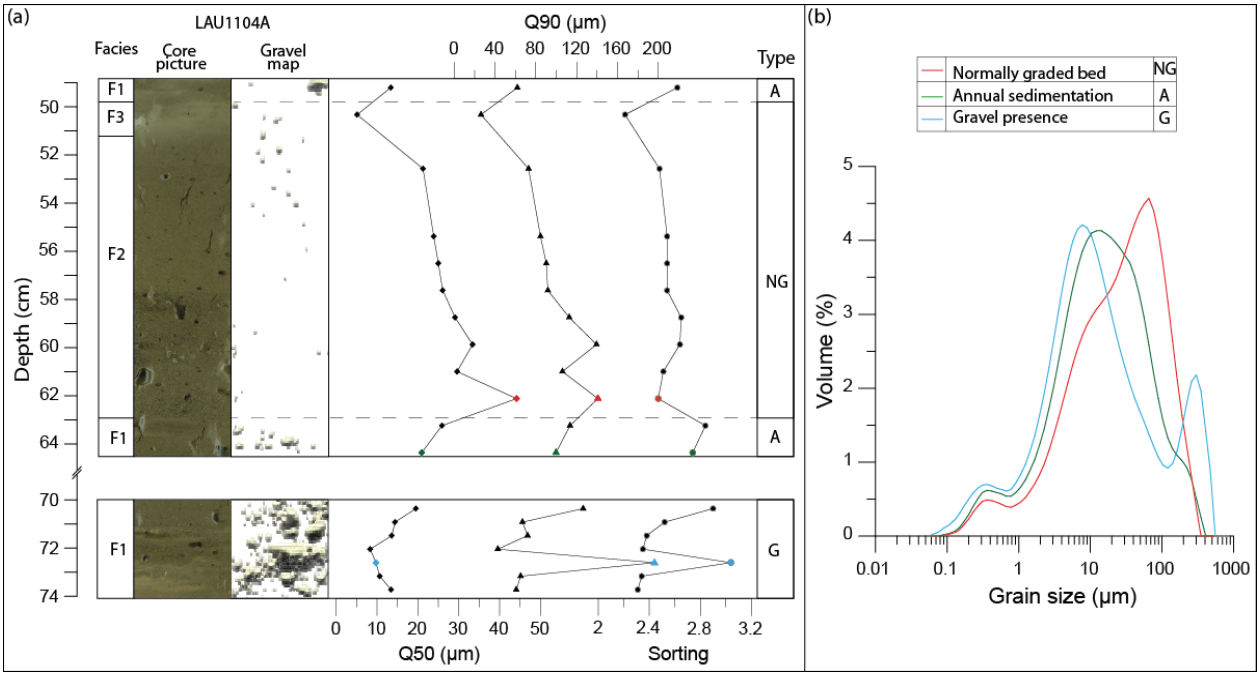

510

Figure 2: (a) Characterization of typical facies of LAU1104A sediment core, based on Median grain size (Q50), 10th percentile coarse grains (Q90) and sorting parameters. (b) Comparison between: NG-normally graded bed base sample (red line); A-annual sedimentation (green line) and G-gravel presence (blue line) grain size distributions

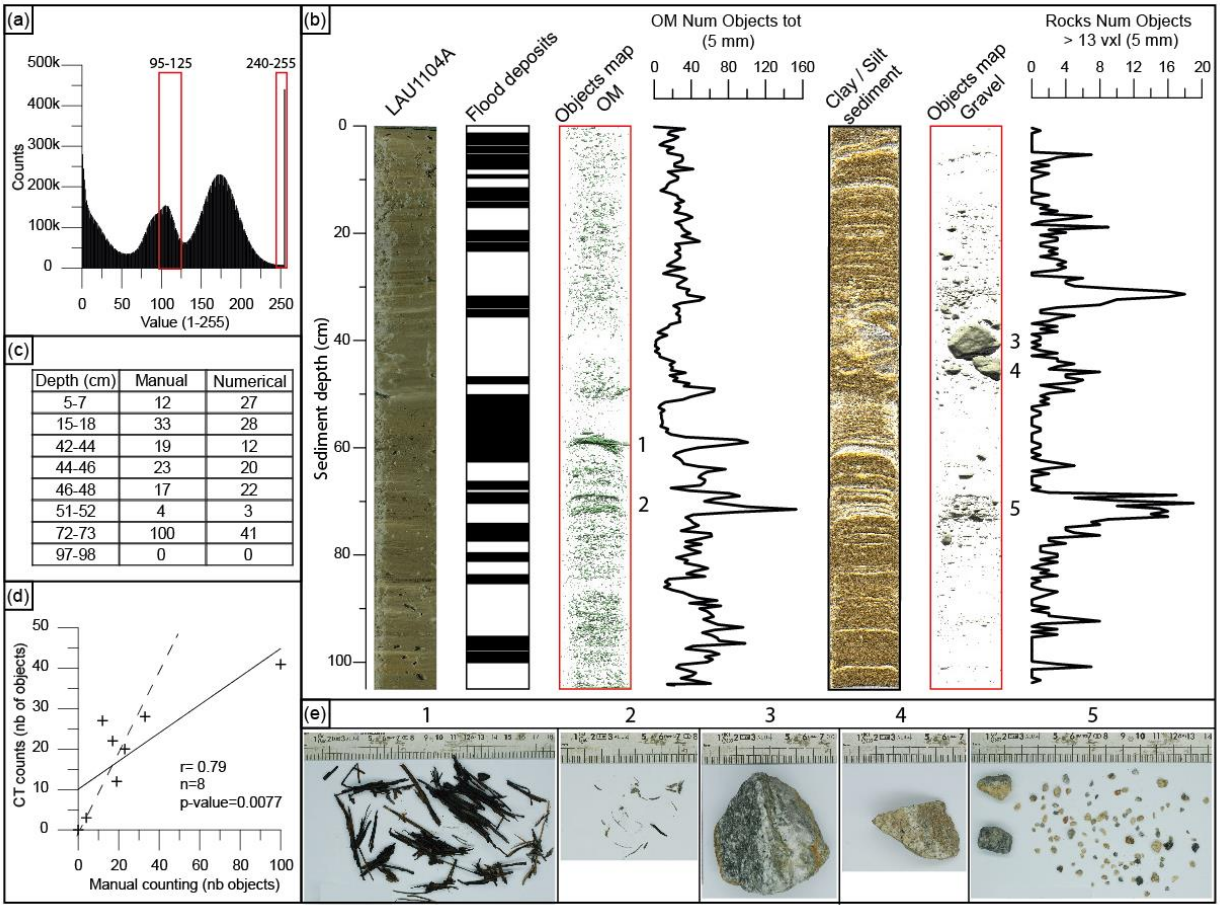

Depth (cm)	Manual	Numerical
5-7	12	27
15-18	33	28
42-44	19	12
44-46	23	20
46-48	17	22
51-52	4	3
72-73	100	41
97-98	0	0

Figure 3: (a) Number of counts histogram for 1 to 255 levels of grey; selected range for OM (95-125) and for gravels (240-255) shown in red. (b) From left to right: core LAU1104A photography, position of flood deposits, CT image stacks of both rocks and OM and corresponding totals summed at 5 mm intervals. (c) Selected depth for comparison between manual and numerical counts in core LAU1104A. (d) Correlation between manual and numerical rock counts (solid line), CT counts=Manual counts (dashed line) (e) Photographs of organic matter (e1, e2) and gravel-sized elements (e3, e4, e5) recovered from the LAU1104 sediment core.

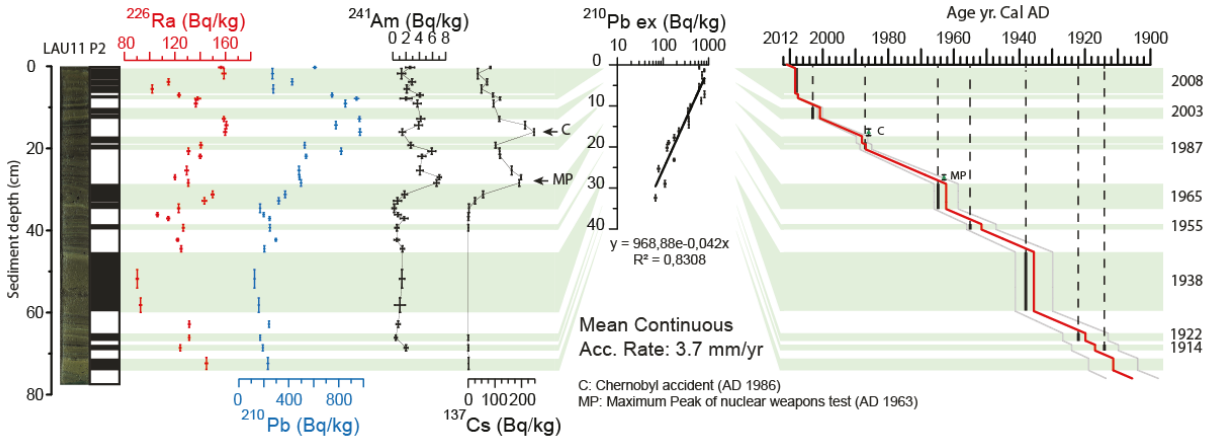

Figure 4: ^{226}Ra, ^{210}Pb, ^{241}Am, and ^{137}Cs activity profiles for core LAU11P2. Application of the CFCS model to the synthetic sedimentary profile of excess ^{210}Pb (without normally graded beds, which are considered to be instantaneous deposits).

Resulting age-depth relationship with 1σ uncertainties and indications of historic flood dates associated with normally graded beds and the two artificial radionuclide markers.

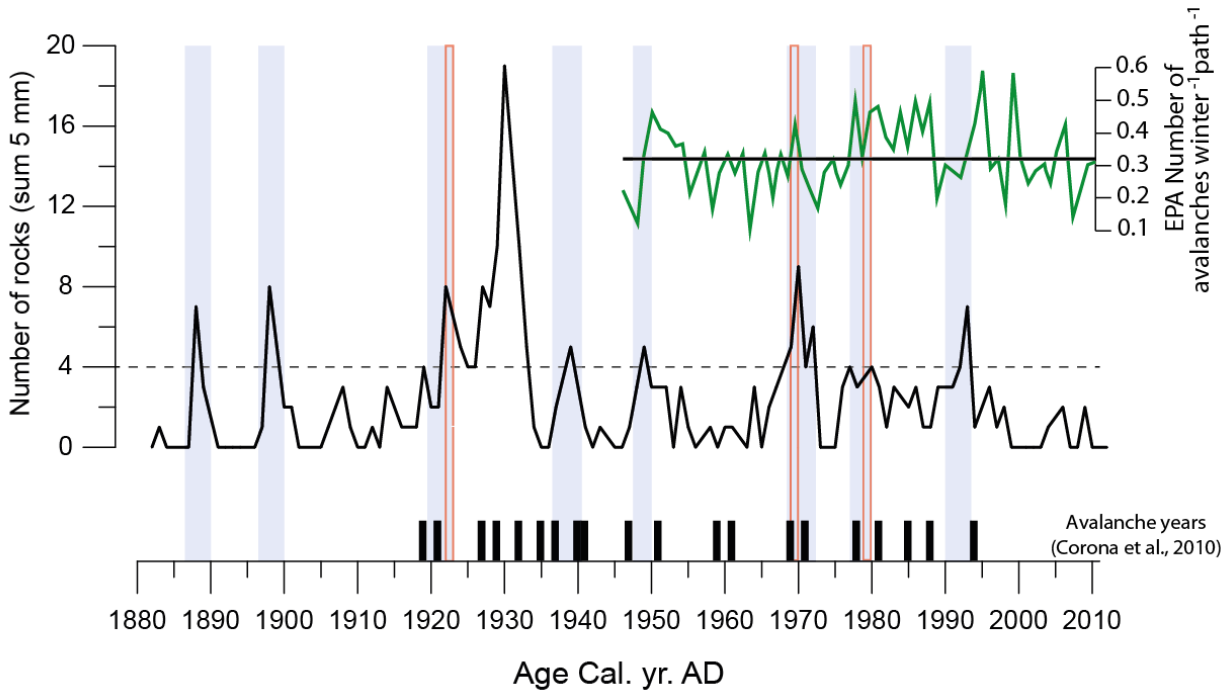

Figure 5: Sum of rocks >13 voxels at 5 mm intervals identified in the LAU1104A sediment core since 1880 Cal. Yr. AD without the normally graded beds. The dashed line represents the threshold number from which avalanche periods are identified (highlighted in blue). Exceptional winters found in the bibliography are represented in red (Allix, 1923; Jail, 1970; Ecrins National Park internal report, 1978). EPA number of avalanches per path since AD 1950 in green, interannual mean value in black (N. Eckert et al., 2013). Avalanche record for the past century from tree rings in the nearby Romanche river valley (Corona et al., 2010).